

Wave-Follower Field Measurements of the Wind-Input Spectral Function. Part III: Parameterization of the Wind-Input Enhancement due to Wave Breaking

ALEXANDER V. BABANIN

Faculty of Engineering and Industrial Sciences, Swinburne University of Technology, Melbourne, Victoria, Australia

MICHAEL L. BANNER

School of Mathematics, University of New South Wales, Sydney, New South Wales, Australia

IAN R. YOUNG

Swinburne University of Technology, Melbourne, Victoria, Australia

MARK A. DONELAN

Rosenstiel School of Marine and Atmospheric Science, University of Miami, Miami, Florida

(Manuscript received 9 January 2007, in final form 16 February 2007)

ABSTRACT

This is the third in a series of papers describing wave-follower observations of the aerodynamic coupling between wind and waves on a large shallow lake during the Australian Shallow Water Experiment (AUSWEX). It focuses on the long-standing problem of the aerodynamic consequences of wave breaking on the wind-wave coupling. Direct field measurements are reported of the influence of wave breaking on the wave-induced pressure in the airflow over water waves, and hence the energy flux to the waves. The level of forcing, measured by the ratio of wind speed to the speed of the dominant (spectral peak) waves, covered the range of 3–7. The propagation speeds of the dominant waves were limited by the water depth and the waves were correspondingly steep. These measurements allowed an assessment of the magnitude of any breaking-induced enhancement operative for these field conditions and provided a basis for parameterizing the effect. Overall, appreciable levels of wave breaking occurred for the strong wind forcing conditions that prevailed during the observational period. Associated with these breaking wave events, a significant phase shift is observed in the local wave-coherent surface pressure. This produced an enhanced wave-coherent energy flux from the wind to the waves with a mean value of 2 times the corresponding energy flux to the nonbreaking waves. It is proposed that the breaking-induced enhancement of the wind input to the waves can be parameterized by the sum of the nonbreaking input and the contribution due to the breaking probability.

1. Introduction

A series of papers from the Australian Shallow Water Experiment (AUSWEX) reports the results of recent measurements of the wind-input source term for wind-generated waves propagating on a finite-depth lake. The special focus of the present paper is on the

analysis and quantification of enhanced energy flux from the wind to the wave field associated with the presence of breaking waves. This effect has been before investigated on the basis of laboratory measurements (e.g., Banner and Melville 1976; Reul et al. 2007; Giovanangeli et al. 1999; Banner 1990, among others) and numerical simulations (Maat and Makin 1992; Kudryavtsev and Makin 2001; Makin and Kudryavtsev 2002), but only recently was detection of the wind-input enhancement in field conditions reported (Young and Babanin 2001; Babanin and Young 2006). It is expected that local airflow separation accompanies wave breaking, causes a phase shift of the wave-induced pressure,

Corresponding author address: Dr. Alexander V. Babanin, Faculty of Engineering and Industrial Sciences, Swinburne University of Technology, P.O. Box 218, Hawthorn, Melbourne, VIC 3122, Australia.

E-mail: ababanin@swin.edu.au

DOI: 10.1175/2007JPO3757.1

and that this significant modification to the near-surface aerodynamics can result in enhanced wave-coherent momentum and energy fluxes from the wind to the waves.

A detailed description of the AUSWEX field measurement site, instrumentation, and measurement techniques is given in Donelan et al. (2005, hereinafter Part I), while Donelan et al. (2006, hereinafter Part II) describes the prevailing environmental conditions and presents important new results on the physics and parameterization of the spectral wind-input source function for the wave field.

One of the major results reported in Part II was the finding that the familiar exponential growth rate parameter (fractional energy increase per radian) depended on the mean steepness of the waves. Another major finding arose in the context of very strong forcing of steep nonbreaking waves, where a condition of “full” separation was observed. In Part II it was argued that full separation occurs when the local surface curvature at the crest becomes too large for the pressure gradient normal to the wave to be able to balance the centrifugal acceleration of the wind layer in contact with the water surface. During full separation of the wind flow over a steep wave crest, the streamlines detach near the steep crest and do not reattach until well up the windward face of the preceding wave toward its crest (Part II). The consequence is that the shear layer, which is normally adjacent to the surface, detaches and moves upward to leave a “dead zone” in the trough region between the crests. Thus, the external flow passes over the wave troughs and the imposed pressure pattern is weaker than in the usual case of nonseparated flow. However, the phase shift of the pressure maximum toward the reattachment point on the windward face of the wave becomes larger. It was not immediately obvious whether the combined effect would cause enhancement or reduction of the dimensionless wind input, but the quantitative estimates exhibited a significant reduction, compared to the estimated input at the same wave frequencies for the same wind forcing if the full-separation effects were not taken into account.

In this regard, the flow separation due to wave breaking considered in the present paper does not correspond to full separation: it does somewhat increase the phase shift of the induced-pressure maximum with respect to the wave trough, but the flow does not pass over the wave troughs altogether as in the case of the full separation. As a result, there is an enhancement rather than reduction of the wave-induced pressure magnitude, plus the increased phase shift, and the flow separation due to breaking was always found to result in enhancement of the wind input, as described below.

Qualitative comparison of the two separation effects is sketched in Fig. 1.

The wind-input source function proposed in Part II was parameterized by wave steepness and degree of separation, in addition to the traditional wind-forcing properties. This formulation was shown to be in agreement with, and in fact to be able to reconcile, previous field and laboratory data obtained for a variety of conditions in terms of wind forcing and wave steepness. Hence the steady-state, strong forcing conditions during AUSWEX have enabled us to define a generalized wind-input source function that is suitable for parameterizing wave amplification through wind action for a wide range of conditions.

Part II also includes a substantial literature review of the rich history of this topic: for the sake of brevity, the interested reader is referred to section 1 in that paper. Further to that review, it should be added that airflow separation underpinned Jeffreys’s (1924, 1925) sheltering hypothesis, one of the early mechanisms proposed for wind–wave generation. Jeffreys’s model was conceived from flow over solid obstacles, for which every boundary point is a stationary point and hence a potential stagnation point. Banner and Melville (1976) and Gent and Taylor (1976) discussed the differences when a free surface boundary is involved. Banner and Melville (1976) argued that wave breaking was sufficient to provide a stagnation point at the breaking crest, in a frame traveling with the wave, with airflow separation occurring in the following downwind trough triggered by the adverse pressure gradient, while Gent and Taylor (1976) pointed out that because of the tangential motion of the surface, the vanishing of the surface shear stress is not sufficient to ensure separation. These arguments do not exclude the possibility of separated flow based on an internal stagnation point, such as has been observed in the flow over a counterrotating cylinder (see Batchelor 1967, his Fig. 6.6.2). Indeed, in Part II, we described what we believe are the first reported field observations of the onset of a separated flow regime associated with wind flow curvature effects over nonbreaking waves, and proposed a spectral wind-input source function that models the strong aerodynamic effects that we observed.

For an established field of wind waves, breaking occurs over a range of wave scales and directions (e.g., Melville and Matusov 2002). Since wave breaking can be very frequent (up to 60% in Babanin et al. 2001), the breaking-induced separation has the potential to produce a noticeable enhancement of the atmospheric input to the waves. Indeed, Kudryavtsev and Makin (2001) and Makin and Kudryavtsev (2002) have parameterized breaking into their phase-resolvent model for

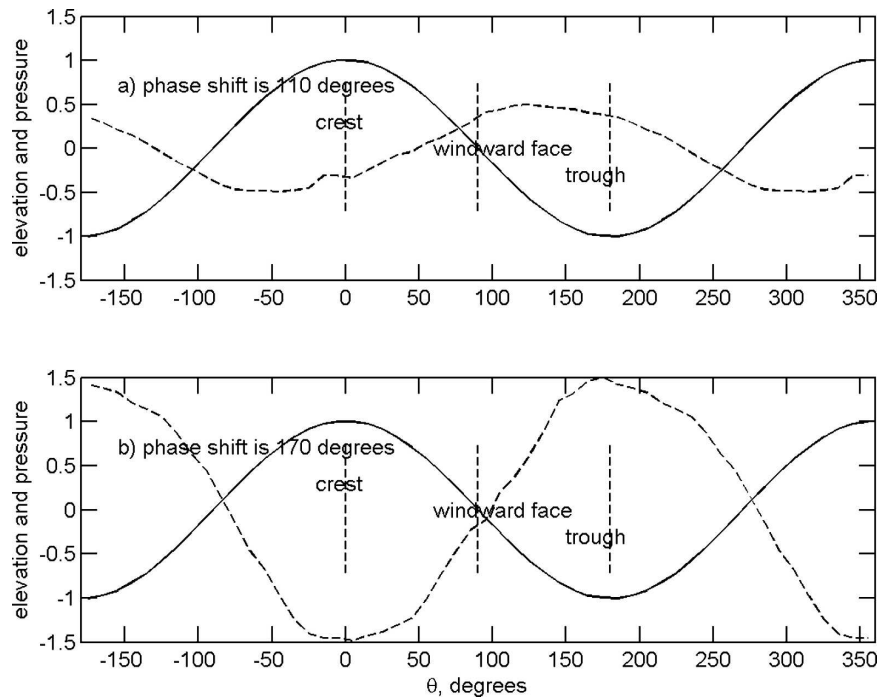


FIG. 1. Illustration of qualitative differences between (a) the full flow separation and (b) separation due to wave breaking. The solid line signifies the surface water wave. Positions of the crest, trough, and windward face of this wave are indicated with the vertical lines. The dashed line demonstrates the induced pressure wave. Vertical scales are arbitrary and vertical dimensions of the pressure waves in (a) and (b) are scaled relative to the water wave.

ocean wind waves and they attribute up to 50% of the total wave-induced stress to breaking. Clearly, such model estimates need to be validated observationally.

The specific aim of this paper is to demonstrate the effect of interfacial energy flux enhancement over breaking waves on the basis of field data and to provide a quantitative assessment in order to develop an appropriate parameterization for its inclusion in wind-wave and air-sea interaction models. The paper is written around five figures, each of which is intended to highlight the enhancement effect from a different perspective. In Fig. 2, the effect is demonstrated. Figure 3 illustrates the procedure we used for routine breaking identification based on a clear detection of the enhancement and it also illustrates a possible dependence of the enhancement on the breaking severity. Figure 4 shows the average enhancement due to breaking across a set of records. Figure 5 looks at the dependence of the effect on the steepness of breaking waves. Figure 6 depicts the enhancement in a phase-average frame locked to the wave profile.

2. Measurements

The measurements were made at the Lake George field experimental site during active wind-generating

situations. The site, environmental conditions, and measurement instrumentation are comprehensively described by Young et al. (2005), and the techniques for extracting the wave-coherent surface pressure of the wind are explained in detail in the companion papers (Part I and Part II), to which the interested reader is referred. Here, we recall that the wave-induced pressure was sensed by Elliott's pressure probes very close to the wavy surface (within a few centimeters) by means of a high-precision wave follower. The prevailing environmental conditions for the set of records analyzed in this paper are summarized in Table 1.

Of particular interest within the present investigation is the breaking-detection methodology, which relied on detecting enhanced acoustic noise at three bottom-mounted pressure sensors attached to the base of the wave gauge array frame. The setup is described in detail in Part I. The breaking waves generate an enhanced acoustic pressure at high frequencies, which was sensed clearly by the collocated hydrophone (e.g., see Babanin et al. 2001; Manasseh et al. 2006, where two different methodologies for breaking detection were investigated). The same pressure was also detected by the pressure probes, and in this paper we rely on a third method that uses these probes. It should be noted that

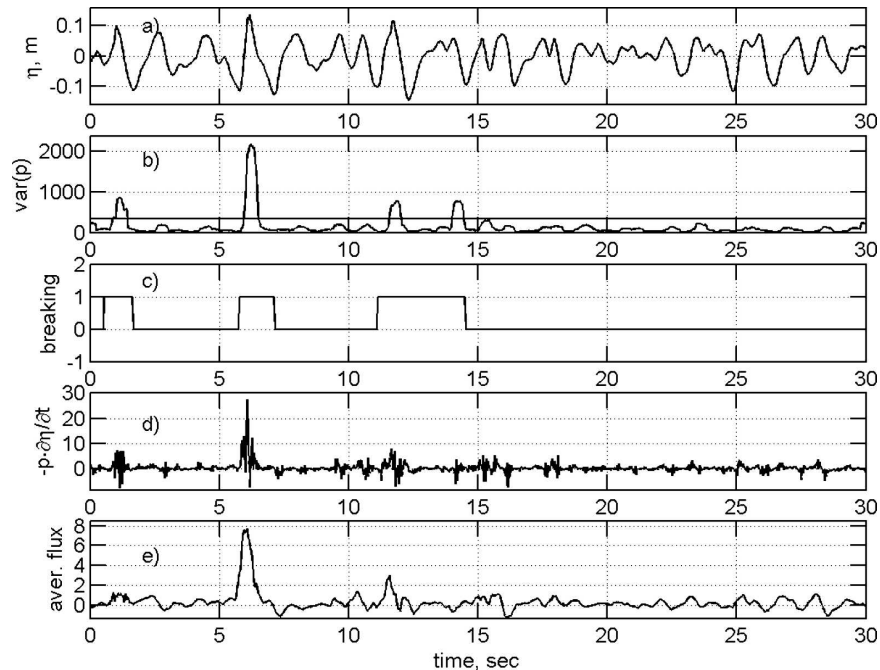


FIG. 2. Representative data illustrating the breaking enhancement. (a) Typical signal of the surface elevation η , measured by the wave resistance wire. (b) Running average of the instantaneous pressure variance $\text{var}(p)$ (high-pass-filtered pressure squared), based on an averaging interval of $0.25/f_p$. Breaking threshold, taken as a factor $b_t = 2.5$ times the run-averaged bottom pressure-squared signal $\text{mean}[\text{var}(p)]$ is shown as the straight line. (c) The unit step function breaking indicator from trough to trough of the wave in (a). Here 0 and 1 correspond, respectively, to “no breaking” and “breaking.” (d) Instantaneous energy flux $p(\partial\eta/\partial t)$. (e) Running average of the energy flux, based on the averaging interval of $0.25/f_p$.

the calibration of the pressure transducer is important, but its depth is not. This is because it does not affect the acoustic noise directly whereas the pressure oscillations due to high-frequency waves are attenuated by the depth. To be certain, we high-pass filtered the pressure-transducer signal at 10 Hz, which is some 10 times above the spectral peak frequency f_p .

We attempted to improve the signal-to-background-noise ratio of the breaking-detection procedure by taking the product of the signals from the three bottom pressure probes. However, not all three bottom pressure probes functioned reliably throughout the data acquisition, so we eventually based the breaking detection on one reliable probe and a consistent threshold for breaking as described below.

Thus, the breaking-detection procedure was based on “hearing” the breaking, but we also verified it by visual means (i.e., by “seeing” the breaking). This was done using video records of waves at the measurement location. The video record was taken at the rate of 25 images per second, the same as the sampling frequency of most of the other measurements. All these measurements were synchronized. Once a breaking event was

registered, we used a zero-crossing analysis to identify that whole wave as a breaker and measured its relevant properties (i.e., period, height, and steepness).

Figure 2 illustrates the phenomenon, which is quantified in the subsequent figures. Figure 2a displays the surface elevation η , measured by the wave resistance wire. In the segment shown, the waves around 2, 7, 12, and 14 s were identified as breaking by repeated viewing of the video record. Figure 2b demonstrates the ability of the bottom pressure probes to detect these same events. In this panel, the running average of the instantaneous pressure variance $\text{var}(p)$ is plotted. This is the square of the high-pass-filtered pressure signal. The averaging interval employed to smooth the instantaneous property was chosen as $0.25/f_p$. The bursts in the bottom-transducer high-frequency pressure at appropriate moments are clearly evident, but require setting a relevant threshold to distinguish them above the background pressure/acoustic noise in order to routinely analyze the breakers. This breaking threshold, taken as a factor b_t times the run-averaged bottom pressure-squared signal $\text{mean}[\text{var}(p)]$, is employed in the middle subplot (Fig. 2c). This panel is a unit-step-

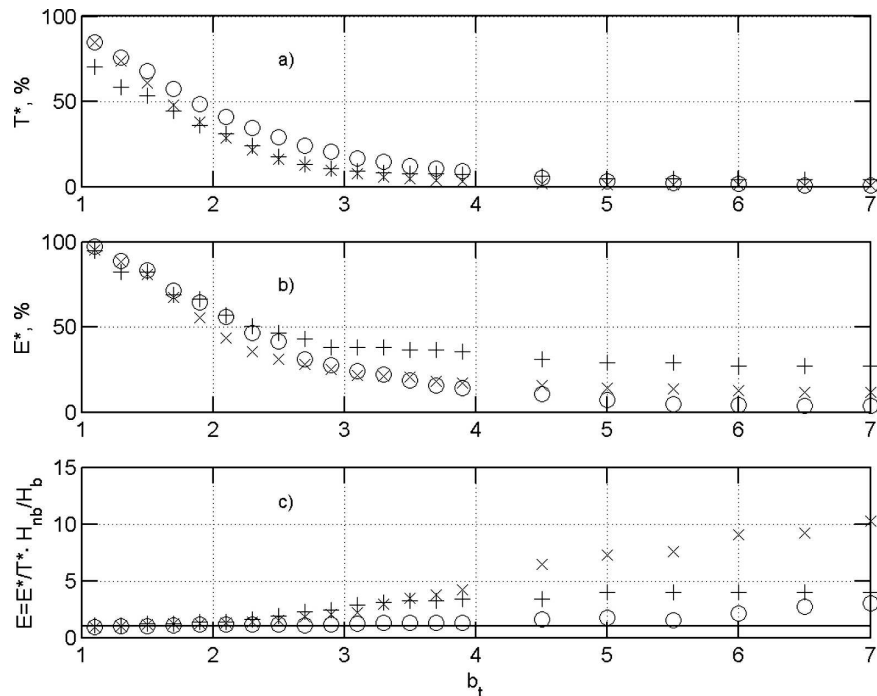


FIG. 3. Basis for the choice of the bottom pressure threshold for registering breaking events. The b_t (bottom scale) is the factor used as a multiplier of the run-averaged bottom pressure-squared signal mean[$\text{var}(p)$]. Data are from record 4 ($U_{10} = 6.6 \text{ m s}^{-1}$; circles), record 10 (8.1 m s^{-1} ; x symbol), and record 8 (11.9 m s^{-1} ; plus signs) of Table 1. (a) The T^* , the observed ratio of breaking duration to total duration. (b) Corresponding dependence of E^* , the relative contribution of breaking waves to the total energy flux. (c) Normalized energy flux enhancement ratio, defined as the ratio of $E^* = E_{br}/E_{tot}$ to $T^* = T_{br}/T_{tot}$.

function breaking indicator—from trough to trough of the wave in the top panel, where 0 indicates no breaking and 1 indicates breaking. For our dataset, b_t was taken as 2.5 throughout the analysis. This choice of b_t was based on the analysis described in section 3a.

In Fig. 2d, the synchronous instantaneous energy flux $p(\partial\eta/\partial t)$ is plotted, where p is the instantaneous pressure detected just above the moving surface and $(\partial\eta/\partial t)$ is the partial time derivative of the elevation η . The wave height signal, which was sampled at $f_s = 50 \text{ Hz}$, was smoothed using a 5-Hz low-pass filter. Again, the bursts are evident, but require a formal averaging procedure to quantify the integral enhanced-pressure effect.

This is done in the next panel, Fig. 2e. To highlight the enhancement effect, this subplot shows the running average of the energy flux, based on the same averaging interval of $0.25/f_p$ as above. It is clear that the flux is enhanced over the second and third breakers, somewhat enhanced over the first one, but hardly at all over the last breaker.

The approach adopted in this paper is based on measuring the flux over breaking waves, the breakers being

detected on the basis of the acoustic noise emitted. The capability of the breakers to emit noise, however, depends strongly on the phase of the wave breaking. Classification of these phases was proposed and discussed in detail in Liu and Babanin (2004). There are four phases: incipient breaking, developing breaking, subsiding breaking, and residual breaking. At the incipient stage, the water surface becomes unstable and the breaking starts, but little if any whitecapping is produced at this stage and therefore the acoustic or visual methods will not detect such a breaker. They will detect it at the developing and subsiding stages when the whitecaps are actively formed, the latter stage being characterized by the originally steep waves having lost much of their height and their steepness has dropped below the mean steepness level. During the last, residual, stage of breaking, whitecaps are left behind, but spatial evolution of mixing continues as the turbulent front is moving downstream (Rapp and Melville 1990)—this stage is not relevant for the present study. Obviously, the first three breakers in Fig. 2a are developing while the last one is subsiding, its steepness being not different to that of nonbreaking waves.

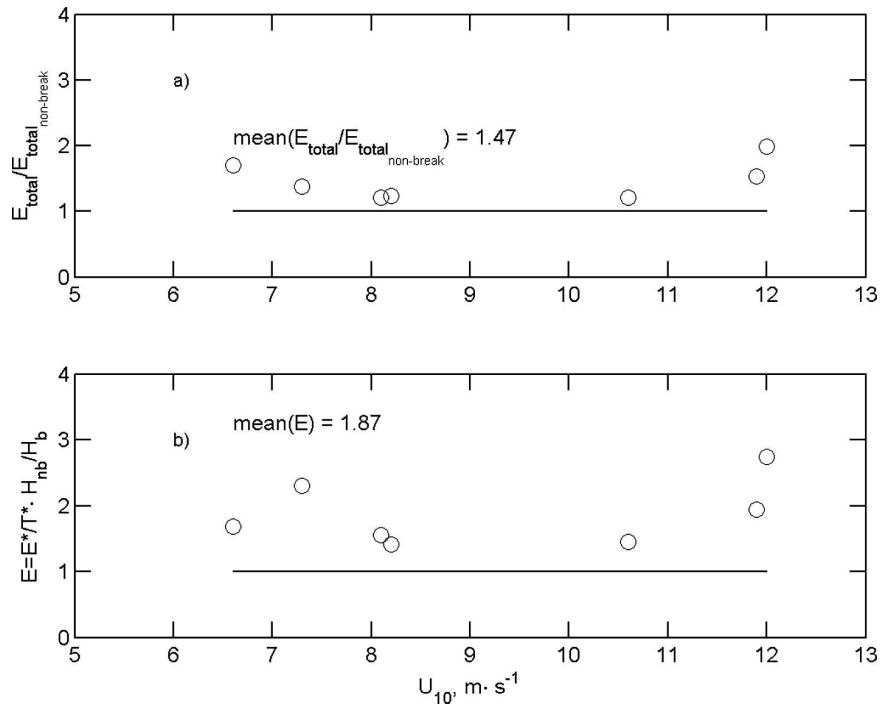


FIG. 4. Measures of breaking enhancement to the wave-coherent energy flux from the wind. (a) Ratio of the total energy flux from the wind to the waves, to this flux in the absence of breaking, as a function of U_{10} . (b) Corresponding results for the breaking enhancement to the wind input E . Note that $E = 1$ for no breaking enhancement.

The enhancement effect is expected to be due to the flow separation over the steep breakers and hence will exhibit itself at the incipient and developing breaking stages, but not at the subsiding and residual stages. Therefore, it is not unexpected that there is no enhancement evident over the fourth breaker in Fig. 2e. This kind of breaker will, however, be routinely detected by means of our acoustic-based technique and will tend to lower the overall enhancement value compared to the integrated energy flux over the entire wave set. Additionally, the acoustic technique will not detect the incipient breakers that may or may not produce a separated flow. If they do, energy fluxes over such waves will be integrated into the contribution of non-breaking waves and thus will lead to underestimation of the breaking-induced enhancement. Therefore, estimates made in the present paper have to be regarded as a lower bound.

3. Results

The choice of the breaking-identification threshold is established in section 3a, and in sections 3b and 3c, this threshold is employed to demonstrate the enhancement effect from different perspectives and to quantify it.

a. Breaking-threshold determination

The basis for our choice of the bottom pressure threshold b_t for registering breaking events is justified in Fig. 3. The datasets used to illustrate this are from three different wind speed cases: $U_{10} = 6.6 \text{ m s}^{-1}$ (record 4; circles), 8.1 m s^{-1} (record 10, x symbols); and 11.9 m s^{-1} (record 8; plus symbols). The bottom pressure signal was processed as described in the previous section.

As mentioned in section 2, the threshold b_t was sought as a multiplier for the run-averaged bottom pressure-squared signal, $\text{mean}[\text{var}(p)]$. When calculated, the product $b_t \cdot \text{mean}[\text{var}(p)]$ identifies a critical value for the running average of the high-pass-filtered bottom pressure signal. If this value is exceeded at any instant, the synchronously recorded wave is considered breaking, its physical properties are determined by the zero-crossing analysis as described above, and the total energy flux over such a local wave is obtained by integration of the instantaneous flux $p(\partial\eta/\partial t)$ from the preceding trough to the following trough. We should mention again that the threshold was chosen such that waves above the critical pressure property were definitely breaking, whereas waves below could possibly have been breaking or nonbreaking. In carrying out this

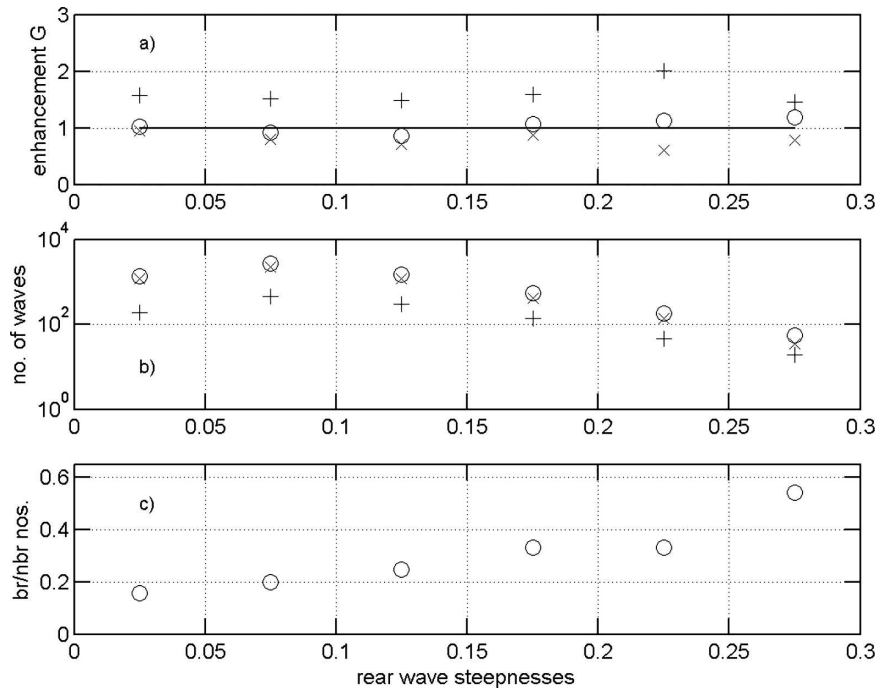


FIG. 5. Key breaking wave statistics and their relative contribution to the energy flux from the wind to the waves. (a), (b) The symbols denote breaking (plus signs), nonbreaking (x symbols), and nonsegregated (circles) waves. (a) Mean enhancement as a function of the rear-face steepness. The energy flux to each individual wave was normalized by its steepness. (b) Statistics derived from counting the waves in each steepness group. (c) Ratio of counted breaking to nonbreaking waves as a function of the steepness of the windward (rear) face of individual waves.

analysis, an iterative procedure was used to suppress the contribution of breaking events to the mean bottom pressure.

The subplots of Fig. 3 demonstrate different wave and wind properties as functions of the magnitude of the chosen b_i value. Figure 3a shows such a dependence for $T^* = T_{br}/T_{tot}$, the ratio of observed breaking duration to total duration. If b_i is chosen very low, all waves will be identified as breaking and the ratio will approach 100%. If b_i is excessively high, no breaking waves will be detected in the record and T^* will asymptote to zero. For high values of b_i well above the threshold but below the ultimate value, the method will select particularly severe breakers, depending on the strength of their acoustic impact.

The acoustic method demonstrates the expected behavior for the breaking duration in general, with noticeable differences between the three wind-forcing situations at low-to-intermediate selected values of b_i . For example, for $b_i = 1$, the method would identify some 80% of waves as breaking at the two lighter winds, but only 70% at the 11.9 m s^{-1} wind. The latter signifies a relatively smaller contribution of particularly “noisy” events to the total noise, which is most likely

caused by a higher level of ambient acoustic noise at strong winds.

Figure 3b shows the corresponding dependence of $E^* = E_{br}/E_{tot}$, the relative contribution of breaking waves to the input energy flux to the waves. It immediately exhibits the expected effect of the enhancement of the wind input. If there was no enhancement of the wind input, the ratio E_{br}/E_{tot} would follow the $T^* = T_{br}/T_{tot}$ dependence, tending to asymptote to zero for severe but rare events. It is clearly not the case for strong breakers with b_i greater than about 2.5, which means that relative contribution of those events to the total flux is greater than their relative duration.

Figure 3c is the most informative subplot in this figure, and underpins our choice of threshold level $b_i = 2.5$. In this panel, plotted as a function of the threshold property b_i , is the ratio $E = E^*/T^*$. This ratio should be 1 for the case when the flux E_{br} had no enhancement compared to the flux that would occur during the period T_{br} if the waves were not breaking. Since the breaking waves usually have larger amplitudes than those not breaking, to avoid any influence of wave steepness on the instantaneous energy fluxes, E_{tot} has been normalized by the significant wave height H_s of

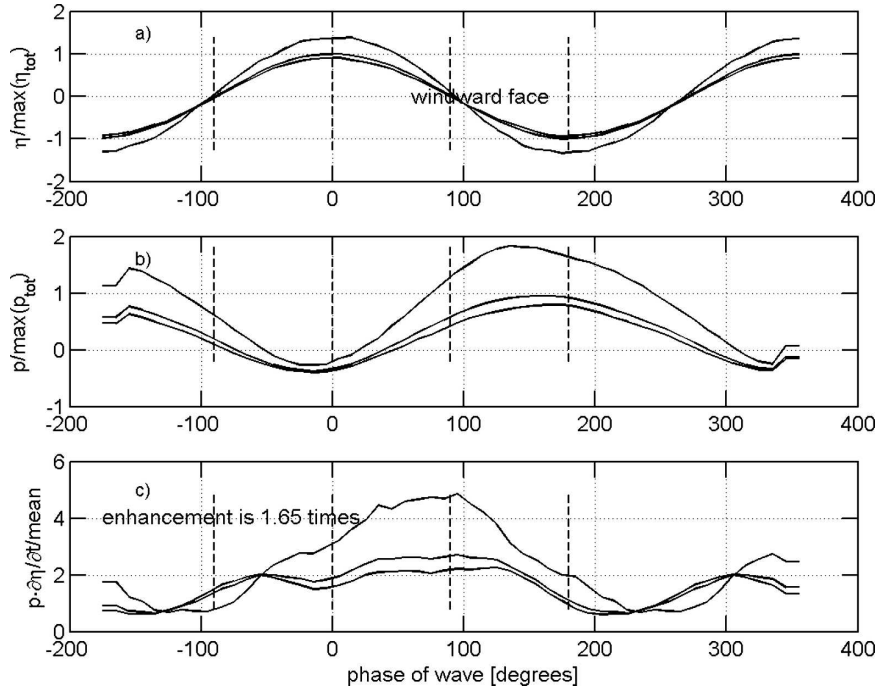


FIG. 6. Phase-averaged breaking enhancement of the wind input for all Part I and Part II records (6347 waves of which 1132 were breaking). Each plot shows the distribution for all waves, for the breakers and for nonbreaking waves. (a) Mean phase-resolved wave profile, (b) surface pressure distribution, and (c) energy flux distribution (all obtained for the 36 phases resolved).

the nonbreaking waves H_{nb} , and E_{br} by the significant wave height of the breaking waves H_b .

The ratio E is seen to be close to or below 1, up to a threshold value of b_t around 2.5, and corresponds approximately to the stage where our threshold starts detecting the breakers and not detecting the nonbreakers. Furthermore, for $b_t = 2.5$, all waves with a bottom pressure exceeding this threshold certainly break. This was verified by viewing the synchronized video imagery for a representative subset of the records. Therefore, this bottom pressure threshold was adopted throughout the analysis to register the breaking waves.

Last, note that waves with acoustic signatures below the bottom pressure threshold of $b_t = 2.5$ may or may not break—the bottom pressure sensing system did not detect breakers reliably near the threshold. That is why the enhancement curves can depart from unity. These data were not taken into account because we wanted to deal with genuinely breaking waves only.

We also point out at this stage that the T^* property of Fig. 3a, taken at $b_t = 2.5$, should not be interpreted as the breaking rate. First of all, as noted above, waves falling below the threshold may or may not break and thus may or may not contribute to the rate. Second, T^* is related to a relative duration of breaking “ringing”

(over the wave period) rather than to a number of breakers, the former being an unknown function of environmental properties such as breaking severity, wind speed, and others. And finally, if T^* is attempted to compare breaking rates for different records, spectral distribution of breaking events may become an issue. For example, if for $U_{10} = 6.6 \text{ m s}^{-1}$, it is mostly peak waves that are breaking and for the other records these are waves above the spectral peak, there will be different duration T^* for the same breaking rate.

Had we adopted a threshold level b_t above 2.5, it would have significantly reduced the breaking occur-

TABLE 1. Environmental conditions of records used. Here, U_{10} is the wind speed at 10-m height, f_p is the peak frequency, and H_s is the significant wave height.

Record No.	U_{10} (m s^{-1})	f_p (Hz)	H_s (m)
4	6.6	1.33	0.05
8	11.9	0.60	0.16
9	12.0	0.52	0.13
10	8.1	0.77	0.08
11	10.6	0.57	0.08
14	8.2	1.12	0.06
15	7.3	0.60	0.07
24	6.4	1.22	0.05

rence rate statistics. As may be seen in Fig. 4b, the number of breaking waves with higher steepness decreases dramatically as the breaking threshold is increased. Thus, the threshold level of 2.5 is a purely empirical level and may only be applicable to this particular experimental setup with the prevailing mean water depth. In deeper water, a different value of b_t could have been needed to detect the breakers reliably if the acoustic-induced pressure above the background noise is reduced for the deep-water breakers.

We should mention that other methods of deriving the breaking-detection threshold were attempted in our search for a universal high-frequency pressure property that would characterize the breaking. In particular, the rms level (averaged over the local wave period) of the high-frequency pressure fluctuations was considered as an indicator of the average breaking intensity over a local wave. It was expected that, if the rms background level of fluctuations at these frequencies in the certain absence of breaking (e.g., during light winds) is subtracted, the remaining property would unambiguously identify the breaking. The background level was obtained from the high-frequency-noise histograms where it should have a high probability. It was found that the extreme values of the high-frequency-noise rms histograms clearly depend on the wind speed, that is, (in arbitrary units) 2.4 for $U_{10} = 6.6 \text{ m s}^{-1}$, 13.1 for $U_{10} = 8.1 \text{ m s}^{-1}$, and 35.8 for $U_{10} = 11.9 \text{ m s}^{-1}$. Mean values of the noise also depend on the wind. Apparently, the background ambient noise at different wind speeds changes due to the presence of small-scale breakers and the detection threshold would have to be determined for each wave record individually.

It is interesting to highlight some consequences of Fig. 3 that are not immediately related to the topic of the present paper. Figure 3c qualitatively shows the dependence of the enhancement effect on the breaking severity, since higher thresholds imply that only more severe breakers are detected. It is apparent that the contribution to the ratio E in Fig. 3c increases for more severe breaking events, implying a dependence of the enhancement on the breaking severity. Another interesting feature is that the enhancement effect increases for stronger winds (record 10), but reduces for the fully separated case (record 8, Part II). Hence there are some additional dependences underlying the mean value of the $O(100\%)$ enhancement indicated from our results.

b. Breaking enhancement to the wave-coherent energy flux from the wind

Figures 4–6 of this section demonstrate different analyses of the flux enhancement effect. In Fig. 4, the

average enhancement for the eight records of Table 1 is shown.

In Fig. 4a, the ratio of the total energy flux from the wind to the waves, to this flux in the absence of breaking, is plotted as a function of the wind speed U_{10} . To determine this ratio, the nonbreaking part of the record was effectively “stretched” to the whole length of the record:

$$E_{\text{totalnon-break}} = E_{\text{non-br}} \left(\frac{T_{\text{tot}}}{T_{\text{non-br}}} \right),$$

where $T_{\text{non-br}}$ is the total duration of nonbreaking segments and $E_{\text{non-br}}$ is the total measured energy flux during the $T_{\text{non-br}}$ period. Values of the ratio for individual records vary from 1.2 to 2.0, with no dependence on the wind speed. Obviously, this ratio will depend on the wave-breaking rates which are a complex function of the wave spectrum and wind speed (Babanin and Young 2005; Manasseh et al. 2006). Therefore the average enhancement plotted in Fig. 4b is a more suitable measure for parameterizing the effect.

Figure 4b shows the corresponding results for the enhancement E . Again, if there were no enhancement, E should be 1 because the relative contribution of the breaking events to the total flux would be the same as their relative duration. We note, however, that a significant mean enhancement of 1.87 was observed, highlighting the potential aerodynamic consequences of wave breaking. Values of E for individual records vary from 1.4 to 2.7, the highest enhancement being exhibited by the most strongly forced waves. This is perhaps connected with the breaking severity as well as with the breaking events as such.

Figure 5 presents further analyses of several key statistics related to breaking waves and their relative contribution to the energy flux from the wind to the waves. Since a dependence of the enhancement on the breaking severity was evident, we investigated a possible dependence of the breaking enhancement on wave steepness. Individual waves were identified by their zero crossings and their windward (rear) face steepness was calculated as

$$\varepsilon = \frac{H}{L},$$

where H is the rear crest-to-trough height and L is the rear crest-to-trough length. Here L was determined from the time series as

$$L = \frac{t_L}{T} \lambda,$$

where t_L is the rear crest-to-trough duration of the wave of period T . The wavelength λ was approximated from the period T on the basis of linear wave theory.

Contributions of the individual waves to the local mean energy flux $p(\partial\eta/\partial t)$ were then estimated. The energy flux to each individual wave was normalized by its rear-face steepness. To calculate the enhancement G for individual waves, this energy flux was divided by the mean energy flux for the entire record, normalized by the significant wave steepness $\varepsilon_s = H_s/(\lambda_p/2)$, where λ_p is the length of waves at the spectral peak:

$$G = \frac{E_{\text{ind}}}{E_{\text{mean}}} \frac{\varepsilon_s}{\varepsilon}.$$

We also examined the influence of normalizing by the wave height. The results were, however, not sensitive to this choice.

Next, the individual waves were segregated into groups according to their steepness. The waves were separated into breaking, nonbreaking, and nonsegregated categories, and then grouped according to their rear-face steepness. The energy flux enhancement for each of these groups was estimated and averaged. This was done for dominant waves from all available Part I and II records. In total, this analysis included 6347 waves, 1132 of which were breaking.

The energy flux enhancement is plotted as a function of the steepness for the complete ensemble in Fig. 5a. The result of this analysis demonstrates that the enhancement does not depend noticeably on the steepness. Thus, once an individual wave of a certain steepness breaks, the mean flux over that wave increases by approximately a factor of 2 compared to the flux over a nonbreaking wave of the same steepness.

A further statistic derived from grouping, and then counting the waves according to their steepness and breaking/nonbreaking characteristics, is shown in Fig. 5b. A semilogarithmic scale was used because the number of waves with large steepness decreases by two orders of magnitude. The distribution according to steepness of Lake George waves has a maximum in the steepness range 0.05–0.1 (2689 waves), and the number of waves rapidly drops toward higher steepness. It is interesting, however, that a significant number (54) of very steep waves, even as steep as 0.25–0.3, were detected.

A variant of this approach, the ratio of counted breaking to nonbreaking waves as a function of the steepness of the windward (rear) face of individual dominant waves, is shown in Fig. 5c. This figure shows the relative probabilities of breakers, conditioned on their rear-face steepness. As one would expect, the larger the wave steepness, the more frequently they break. The ratio reaches 54% for waves in the steepness range 0.25–0.3 (the percentage of breaking waves,

if defined as ratio of the number of breakers to the total number of waves, is 35%).

c. Phase-averaged viewpoint

The phase-average technique, described and widely utilized in Part II, provides interesting and instructive insight into the behavior of wave-induced pressure fluctuations relative to the surface waves. It is a powerful data analysis tool, operative at frequencies and signal-to-noise ratios well beyond the limit where cospectral analysis fails to find any correlation between two related signals.

Figure 6 shows the breaking enhancement of the wind input to the waves from a phase-averaged perspective. In all the subplots, the upper lines are phase averages for 1132 breakers, lower lines are for 5215 nonbreaking waves, and the middle lines are for the nonsegregated 6347 waves.

Hilbert transform analysis was used to determine the phase of the individual dominant waves. This required bandpass filtering the wave height signal around the spectral peak f_p in the spectral band $f_p \pm 0.1f_p$. We note that bandpass filtering changes the wave height and steepness significantly, and this is important here, particularly for the breakers, which are strongly asymmetric and hence are smoothed the most by the bandpass filtering. After determining the phases, the original wave records were used rather than the bandpass-filtered signals.

Once the time series of phases of individual dominant waves had been obtained, the same zero-crossing methodology as in section 3b was applied to single out individual waves. For each wave, the instantaneous phases over the wave profile were placed into one of 36 groups, covering the entire 360°, and the instantaneous flux, wave elevation, and pressure were registered for each phase group. Analyzing all individual waves, the distribution of the average energy flux, the average wave profile, and the average air pressure were obtained for the 36 phases.

Figure 6a shows the mean phase-resolved wave profile for the 36 phases resolved. As expected, the average breaking wave is significantly higher and steeper than the average wave whereas the average nonbreaking wave is marginally lower. It is interesting to note that the phase-average profile of the breaker does not exhibit a noticeable asymmetry of the wave with respect to the vertical.

The phase-average profile of the pressure induced by the breaking wave, however, is very asymmetric (Fig. 6b). While the wave-induced pressure profiles for nonbreaking and nonsegregated waves exhibit an evident shift of the pressure maximum toward the windward

wave face, which we would expect for the strongly forced Lake George waves, the shift in the asymmetric breaking-induced profile is much greater. The magnitude of the breaking-induced pressure is also much larger. Together, this leads to the overall breaking-induced flux enhancement demonstrated in Fig. 6c. This is of order 2 when integrated over the phase-average profile. Again, as in Fig. 5, the flux normalization was done on the basis of the windward face steepness.

4. Discussion, conclusions, and parameterization of the breaking influence

We have analyzed a unique air–sea interaction dataset gathered using a wave-follower during the AUSWEX campaign on Lake George. A significant phase shift in the local wind pressure signal was detected that was clearly associated with wave-breaking events.

These results provide strong field support for the proposition that local airflow separation accompanies local wave-breaking events. Moreover, these strong modifications can result in significant enhancement to the energy flux from the wind to the wave field. The mean level of the enhanced input to the waves was found to be of order 2. We then investigated whether this enhancement had a dependence on wind speed and the wave steepness and how the enhancement was distributed over the surface wave profile.

The parameterization of the nonbreaking wind input is addressed in our companion paper Part II, and applies to a spectrum of wind waves. In regard to parameterizing the input associated with breaking waves, it is important to note that the findings in Figs. 5 and 6 are based on the observed behavior of the dominant wind waves. The results shown earlier in Figs. 3–4 were, however, obtained for any waves that could be determined by a zero-crossing analysis, which here included waves of up to 2 times the dominant wave frequency (Manasseh et al. 2006). If we adopt a standard mean value of 2 times the mean flux for the energy flux enhancement, then we propose that this breaking-induced enhancement of the wind input to the waves can be parameterized as the product of the nonbreaking input with this factor of 2. This contribution then needs to be weighted by the breaking probability for these waves.

It should also be noted that the results here were obtained for waves propagating in a finite-depth lake, under strong wind-forcing conditions. While the present study has shown clearly that airflow separation is operative for such breaking waves, it would be desirable to verify directly that this same effect is also op-

erative for short breaking waves riding on much longer nonbreaking waves, a commonly observed occurrence at sea. This will require an open-ocean version of a wave-following, near-surface aerodynamic-pressure measurement system, which is a particularly challenging measurement to make successfully.

In the meantime, we propose that the effect can be parameterized across the spectrum according to the mean observed breaking augmentation of the nonbreaking energy flux from the wind by a factor of 2 and the breaking probability:

$$\gamma = \gamma_0(1 + b_T),$$

where γ_0 is the spectral wave growth rate increment in the absence of wave breaking and b_T is the associated breaking probability (ratio of the number of breaking crests to the total number of crests at a particular frequency). Here, γ , γ_0 , and b_T are spectral functions [see Part II and Babanin et al. (2001) for detailed definitions]. In this regard, recent papers by Banner et al. (2002), Babanin and Young (2005), and Manasseh et al. (2006) discuss the problem of wave breaking in the spectrum based on field-breaking-wave observations over a range of spectral scales.

Acknowledgments. The authors gratefully acknowledge the financial support for this study from the U.S. Office of Naval Research (Grants N00014-97-1-0234, N00014-97-1-0233, and N00014-00-1-0012) and the Australian Research Council (Grant A00102965). We also express our gratitude to the staff of the School of Civil Engineering of the Australian Defence Force Academy for their help during AUSWEX, particularly to Michael Jones, Mary Dalton, and John MacLeod who provided highly professional and timely logistical support.

REFERENCES

- Babanin, A. V., and I. R. Young, 2005: Two-phase behaviour of the spectral dissipation of wind waves. *Proc. Ocean Waves Measurement and Analysis, Fifth Int. Symp. WAVES2005*, Madrid, Spain, Centro de Estudios y Experimentación de Obras Públicas, Paper 51, 11 pp.
- , and —, 2006: Experimental source terms for spectral wave forecast models. *Proc. Third Chinese-German Symp. Coastal and Ocean Engineering*, Tainan, Taiwan, National Cheng Kung University, 49–60.
- , —, and M. L. Banner, 2001: Breaking probabilities for dominant surface waves on water of finite constant depth. *J. Geophys. Res.*, **106**, 11 659–11 676.
- Banner, M. L., 1990: The influence of wave breaking on the surface pressure distribution in wind-wave interactions. *J. Fluid Mech.*, **211**, 463–495.
- , and W. K. Melville, 1976: On the separation of air flow above water waves. *J. Fluid Mech.*, **77**, 825–842.
- , J. R. Gemmrich, and D. M. Farmer, 2002: Multiscale mea-

- surements of ocean wave breaking probability. *J. Phys. Oceanogr.*, **32**, 3364–3375.
- Batchelor, G. K., 1967: *An Introduction to Fluid Dynamics*. Cambridge University Press, 615 pp.
- Donelan, M. A., A. V. Babanin, I. R. Young, M. L. Banner, and C. McCormick, 2005: Wave-follower field measurements of the wind-input spectral function. Part I: Measurements and calibrations. *J. Atmos. Oceanic Technol.*, **22**, 799–813.
- , —, —, and —, 2006: Wave-follower field measurements of the wind-input spectral function. Part II: Parameterization of the wind input. *J. Phys. Oceanogr.*, **36**, 1672–1688.
- Gent, P. R., and P. A. Taylor, 1976: A numerical model of the air flow above water waves. *J. Fluid Mech.*, **77**, 105–108.
- Giovanangeli, J. P., N. Reul, M. H. Garat, and H. Branger, 1999: Some aspects of wind-wave coupling at high winds: An experimental study. *Wind-over-Wave Couplings*, S. G. Sajjadi et al., Eds., Oxford University Press, 81–90.
- Jeffreys, H., 1924: On the formation of waves by wind. *Proc. Roy. Soc. London*, **107A**, 189–206.
- , 1925: On the formation of waves by wind. II. *Proc. Roy. Soc. London*, **110A**, 341–347.
- Kudryavtsev, V. N., and V. K. Makin, 2001: The impact of air-flow separation on the drag of the sea surface. *Bound.-Layer Meteor.*, **98**, 155–171.
- Liu, P. C., and A. V. Babanin, 2004: Using wavelet spectrum analysis to resolve breaking events in the wind wave time series. *Ann. Geophys.*, **22**, 3335–3345.
- Maat, N., and V. K. Makin, 1992: Numerical simulation of air flow over breaking waves. *Bound.-Layer Meteor.*, **60**, 77–93.
- Makin, V. K., and V. N. Kudryavtsev, 2002: Impact of dominant waves on sea drag. *Bound.-Layer Meteor.*, **103**, 83–99.
- Manasseh, R., A. V. Babanin, C. Forbes, K. Rickards, I. Bobevski, and A. Ooi, 2006: Passive acoustic determination of wave-breaking events and their severity across the spectrum. *J. Atmos. Oceanic Technol.*, **23**, 599–618.
- Melville, W. K., and P. Matusov, 2002: Distribution of breaking waves at the ocean surface. *Nature*, **417**, 58–63.
- Rapp, R. J., and W. K. Melville, 1990: Laboratory measurements of deep-water breaking waves. *Philos. Trans. Roy. Soc. London*, **311A**, 735–800.
- Reul, N., H. Branger, and J. P. Giovanangeli, 2007: Air flow structure over short breaking waves. *Bound.-Layer Meteor.*, in press.
- Young, I. R., and A. V. Babanin, 2001: Wind wave evolution in finite depth water. *Proc. 14th Australasian Fluid Mechanics Conf.*, Adelaide, Australia, Adelaide University, 79–86.
- , M. L. Banner, M. A. Donelan, A. V. Babanin, W. K. Melville, F. Veron, and C. McCormick, 2005: An integrated study of the wind wave source term balance in finite depth water. *J. Atmos. Oceanic Technol.*, **22**, 814–828.